



Investigating Temperature Variations of Solar Corona during Coronal Mass Ejections

Master's thesis submitted by

Dheeraj Vittal Shenoy

USN: 22MSRPH022

Under the guidance of

Mr. Sundar M. N.

and

Dr. Tanmoy Samanta

To

Department Of Physics and Electronics

School Of Sciences, JAIN (Deemed-to-be University)

Bengaluru

April 2024

ACKNOWLEDGEMENT

I would like to express my sincere gratitude to **Mr. Sundar M. N.** and **Dr. Tanmoy Samanta** for their invaluable guidance and support throughout my project. Their expertise has been instrumental in my success. I am truly grateful for their contributions and the knowledge I have gained under their mentorship.

I would like to specially thank **Indian Institute of Astrophysics (IIA)**, Koramangala, Bengaluru for letting me use their library for study purpose and also their internet facility during my time spent in the campus for this project.

I am also grateful to **Dr. Asha Rajiv**, Director, School of Sciences, **Dr. K. N. Varalakshmi**, Director, Centre for Research in Pure & Applied Sciences and **Dr. S. A. Hariprasad**, Dean Academics, JAIN (Deemed-to-be University) for providing us with this opportunity. I am thankful to **Dr. Sudhakara Reddy**, Head of the Department of Physics and Electronics and **Dr. N. Shanthi**, Program-Head, M. Sc. Programme, for their constant support and encouragement.

I thank **Dr. Chenraj Roychand**, Chancellor, **Dr. N. Sundararajan**, Pro-Chancellor, **Dr. Jithendra Kumar Mishra**, Registrar and **Dr. Raj Singh**, Vice-Chancellor, JAIN (Deemed-to-be University) for providing the required infrastructure and support without which this project would not have been possible.

I am grateful to all the faculty members, Mr. Arvind Krishnapur, Physics lab technician and Mr. Rajesh, Physics lab assistant for their kind support towards us.

(Dheeraj Vittal Shenoy)

April, 2024

Bengaluru

Contents

1	Abstract	1
2	Introduction	2
2.1	Sun	2
2.2	Structure of the Sun	3
2.3	Solar Corona	3
2.4	Solar Flares	4
2.5	Coronal Mass Ejections (CMEs)	5
2.6	Stellar CMEs	6
2.7	Coronal Dimming	7
2.8	Instrument	8
3	Literature Review	11
4	Methodology	12
4.1	Data Analysis tools used	13
4.2	Event Selection	13
4.3	Data	15
4.4	Image Pre-Processing	15
4.5	DEM Analysis	16
4.5.1	Emission Measure	17
4.5.2	Differential Emission Measure	17
4.5.3	Differential Emission Measure Inversion	18
4.6	Data Analysis Procedure	19
5	Results	21
6	Discussion and Conclusion	25

List of Figures

1	Structure of the Sun	3
2	Image of Solar corona during a total solar eclipse	4
3	Solar flare (4 th August 2011)	5
4	Filament and Prominence	6
5	Extrapolation of Solar flare-CME relation	7
6	AIA images of Coronal Dimming regions on the Sun	8
7	SDO Spacecraft	9
8	AIA telescope and it's Layout	10
9	AIA Temperature Response Curves	11
10	Image of the Earth to scale of the 2012 August	14
11	SOHO/LASCO C2 running difference images of the selected events	14
12	SOHO/LASCO C2 images with AIA 193 Å filter	15
13	DEM full disk image of Sun	20
14	Full disk and pointified image of Sun	21
15	DEM Timeseries for 4 th August 2011 Event	22
16	DEM Timeseries for 31 st August 2012 Event	22
17	DEM Timeseries for 28 th October 2021 Event	22
18	DEM profile for 4 th August 2011 event	24
19	DEM profile for 31 st August 2012 Event	24
20	DEM profile for 28 th October 2021 event	24

Abbreviation	Full Form
SDO	Solar Dynamics Observatory
AIA	Atmospheric Imaging Assembly
HMI	Helioseismic Magnetic Imaging
EVE	Extreme ultraviolet Variability Experiment
SOHO	Solar and Heliospheric Observatory
LASCO	Large Angle and Spectrometric Coronagraph Experiment
EUV	Extreme Ultra Violet
DEM	Differential Emission Measure
JSOC	Joint Special Operations Command
FITS	Flexible Image Transport System
SSW	Solar SoftWare
IDL	Interactive Data Language
DN	Data Number
FOV	Field of View
CCD	Charge Coupled Devices
RML	Regularized Maximum Likelihood
GLE	Ground Level Enhancement

Table 1: List of abbreviations

1 Abstract

Coronal Mass Ejections (CME) are expulsions of plasma from the Sun's corona into the heliosphere due to magnetic reconnection. The study investigates the temperature variations of solar corona during CME events on the Sun through a differential emission measure (DEM) analysis. Leveraging data from Atmospheric Imaging Assembly (AIA) of Solar Dynamics Observatory (SDO), we apply DEM inversion technique to derive the temperature distribution of coronal plasma. We analyse three distinct CME events on the Sun, each associated with unique solar phenomena. The first event is characterized by Coronal Dimming, a phenomena linked to the mass loss from the solar corona. The second event is associated with a large filament eruption and the third event is a ground-level enhancement CME event. In addition to traditional DEM analysis, we investigate which temperature plasma exhibits the most significant dimming during CME events which are associated with coronal dimmings. By correlating the dimming intensity with temperature, we identify the temperature range associated with the most pronounced dimming, providing valuable information on the underlying physical mechanisms driving coronal dimming phenomena. Using an approach of converting full disk image into a point source, we conduct DEM analysis to examine the temperature distribution of the point source and compare it to the full disk image DEM. A good correlation is found in DEM curves of the point source and full disk source through DEM analysis in the temperature range of $\log T = [5.85, 6.45]$. This means that the point source converted Sun shows characteristic signatures showed by full disk Sun during coronal dimming, filament eruption and Groundlevel Enhancement CME below $\log T \leq 6.45$.

Keywords: Solar Physics, Coronal Mass Ejections, Atmospheric Imaging Assembly (AIA), Differential Emission Measure (DEM)

2 Introduction

In this section, we will look at the structure of Sun and then proceed to eruptive events like Solar flares, Coronal Mass Ejections, Stellar Coronal Mass Ejections, Coronal Dimming.

2.1 Sun

The Sun is a conspicuous and important celestial body that provides Earth with its primary heat, light, and energy supply as well as acting as the gravitational anchor for our solar system. It is a yellow dwarf, or G-type main-sequence star, that is located at the heart of our solar system. Knowing the Sun is essential to understanding the dynamics of our planetary system, as well as to obtain knowledge of basic astrophysical processes and the properties of stars in the larger universe. Sun is a massive object that makes up around 99.86% of the solar system's total mass. With a diameter of roughly 1.4 million kilometers, it is roughly 109 times bigger than Earth. In comparison to the enormous diversity of stars in the cosmos, the Sun is regarded as an average-sized star despite its enormous size.

Sun is an essential component of keeping life on Earth alive. Its emission of energy affects weather patterns, ocean currents, and ecosystems, driving the planet's climate. Photosynthesis, the process by which plants turn carbon dioxide into oxygen and build the base of the food chain, is made easier by sunlight. The steady orbits of planets in our solar system are also maintained by the gravitational pull of the Sun.

Our knowledge of the Sun has greatly increased because to scientific tools and satellite missions like the Solar and Heliospheric Observatory (SOHO), the Solar Dynamics Observatory (SDO), and most recently, Aditya-L1. With the use of these instruments, scientists are able to track solar activity, detect solar phenomena, and investigate the Sun's effects on the solar system and beyond.

2.2 Structure of the Sun

Sun is divided into three regions, namely, interior region, visible surface and atmosphere. The interior region is further divided into core, radiative zone and convective zone. The **core** is the main fuel station for Sun, where nuclear fusion process is converting H to He. The radiations produced during the fusion process escapes through the surface as visible light. The **radiative zone** extends from the outer edge of the core to the base of the convective zone. Figure 1 shows the structure of Sun. The layer that separates the Sun's interior and its atmosphere is called as **photosphere**. The outer atmosphere of the Sun is called the **corona**, which is a source of solar wind. The inner atmosphere of the Sun is known as the **chromosphere**. Because of the high hydrogen content, Sun appears red when viewed through a solar telescope, hence the name chromosphere.

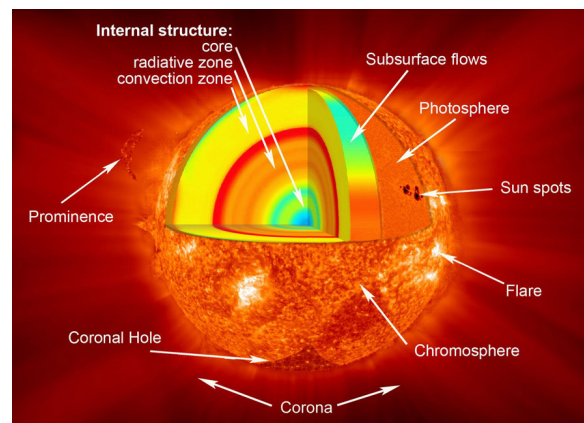


Figure 1: Structure of Sun. (Image credit: NASA)

The radiations produced in the core radiates slowly outwards through this region into the convective zone, taking more than about 170,000 years to radiate through this layer. The **convective zone** is the region where the plasma, through the process of convection currents of heated and cooled gas, moves towards the surface.

2.3 Solar Corona

Outermost layer of the Sun's atmosphere is known as Solar Corona. It lies above the chromosphere and extends millions of kilometers into outer space. Corona can be easily viewed

during solar eclipse (fig. 2), but can also be observed using a coronagraph. Coronagraph is a device that occults the disk of the Sun (similar to how moon occults the Sun during solar eclipse) thereby enabling easy coronal observations and analysis.

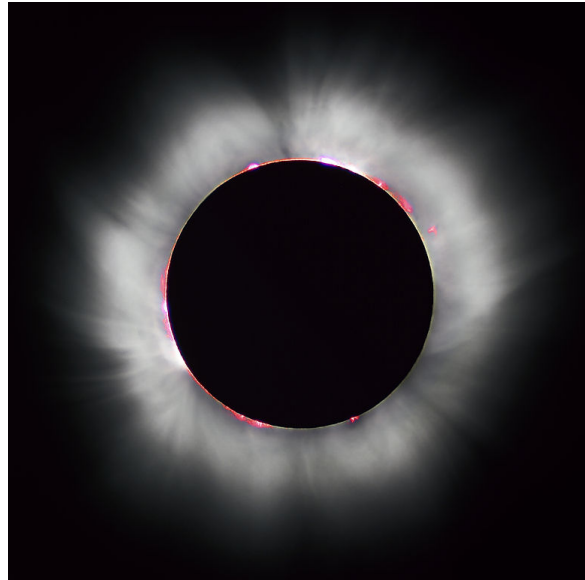


Figure 2: Image of Solar corona during a total solar eclipse. (Image credit: NASA)

The temperature of solar corona is of the order of million of degree kelvin. The emitted plasma can be seen in the EUV region and it is possible to observe the corona using EUV filters without a coronagraph. The unusual spectral features of the solar corona have been explained by the existence of (Fe-XIV or Fe^{13+}). (Aschwanden, 2006)

2.4 Solar Flares

Explosive phenomenas that occur on the surface of sun are called as solar flares, caused by the reconnection of a sun's magnetic field lines. These flares are often accompanied by filaments/prominent eruptions and Coronal Mass Ejections (CMEs). Flares are classified into two types: *eruptive* and *confined*. Eruptive events are the flares which are associated with CMEs and confined flares are those which are not associated with CMEs. Plasma and magnetic field structures sometimes extend outwards from the surface. These structures are called filaments/prominences. Filaments and prominences are fundamentally of the same

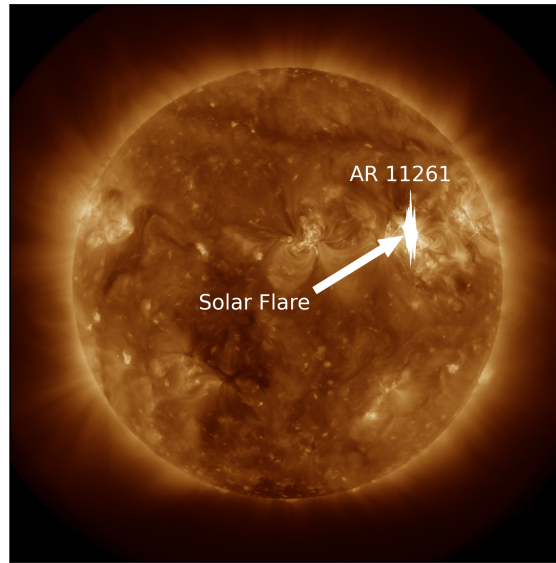


Figure 3: Solar flare event of 4th August 2011 originating from the Active Region AR 11261 observed through 193 Å AIA channel

physical properties, only difference is the angle at which it is observed. If plasma floats outside the solar limb, it is called prominence, it is called a filament if it is within the solar background otherwise fig. 4. Difference is in the type of spectrum obtained, which is Balmer lines in emission spectra in case of prominences and absorption lines in case of filaments. Loop-like structures of plasma stand out brightly against the dark background of space, these are prominences. An image of solar flare event of 4th August 2011 is shown in fig. 3.

2.5 Coronal Mass Ejections (CMEs)

CMEs are large plasma structures ejected from the solar surface to the heliosphere. They were first discovered in 1971 (Gopalswamy, 2016). They majorly affect the space weather, causes interplanetary disturbances and shock waves. CMEs propagating towards the earth can disrupt the communication technologies like satellites. Filament eruptions and solar flares are often associated with CMEs. These energetic plasma have energy of the order of $10^{29} - 10^{32}$ erg and fast speeds even up to 3600 km s^{-1}

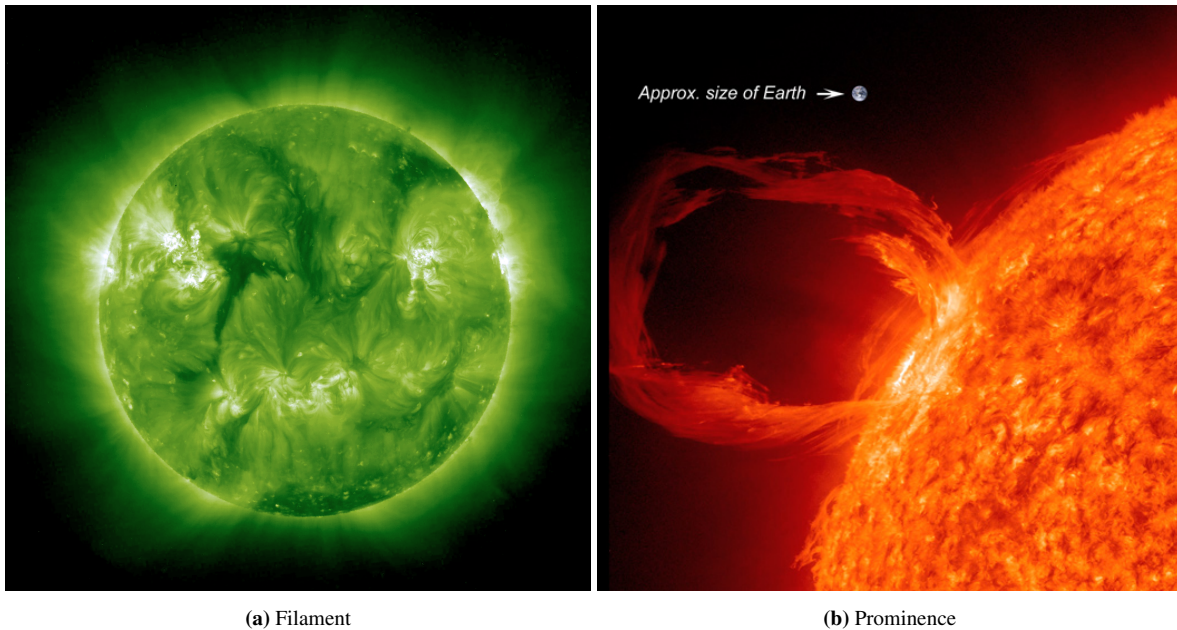


Figure 4: Figure 4a shows a U-shaped very long filament which was stable for a period of two days (6th - 7th February 2012) . Figure 4b is a prominence eruption seen in Extreme UV light on 30th March 2010 (credit: NASA).

2.6 Stellar CMEs

Similar to solar flares, stellar flares maybe associated with CMEs, but it is not easy to detect or study them as there is no spatial resolution unlike Sun. CMEs accompanied by stellar flares are substantially larger in comparison to the ones observed on the Sun, and have been known to affect the exoplanets around the host stars ([Veronig et al., 2021](#)). Hence studying the CMEs is very crucial for future exoplanetary expeditions also. Indirect stellar CME detections have been explored with methods such as coronal dimming, blueshifted emission of chromospheric lines, X-ray, EUV and FUV dimming, Type-II and type-IV radio bursts etc ([Korhonen et al., 2016](#)). Conceptually, stellar CMEs energetics might be thought of as an extrapolation of case of solar CME. But, ([Argiroffi et al., 2019](#)) found that the ratio of stellar CMEs to the flaring energy is not found to be extrapolated version of solar case as seen in fig. 5.

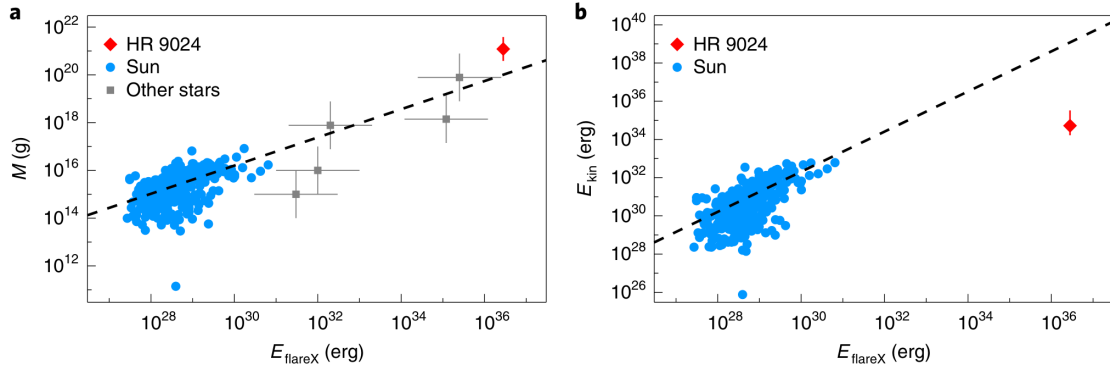


Figure 5: Extrapolation of the solar flare-CME relation. Mass and kinetic energy of solar CMEs shown as a function of X-ray fluence of the associated flares. (Argiroffi et al., 2019)

2.7 Coronal Dimming

Coronal dimming is considered one of the promising signatures to detect the occurrence of stellar CMEs (Namekata et al., 2022). Regions with temporary dimming of plasma on the solar surface is seen after an eruptive event like CMEs in the EUV and soft X-ray wavelengths. This dimming observed is due to the mass loss in the corona after an eruptive event like CME (Mason et al., 2014). Dimming is most prominently observed in the 1-2 million K range of Sun's plasma of the quiet corona. Time series plot of irradiance value of Sun shows a prominent decrease after the event compared to the value before the event. This effect is known as Coronal Dimming. The probability of Coronal Dimming being associated with CMEs have been observed to be very high $P(\text{Dim} | \text{CME}) = 0.842$ in comparison to false alerts $P(\text{Dim} | \neg \text{CME}) = 0.167$. Probability of CMEs being associated with dimming ($P(\text{CME} | \text{Dim}) = 0.970$) is also very high (Veronig et al., 2021). Many studies have been done to get information about the underlying CME from the coronal dimming. The depth and slope of the dimming region in the light curve during CME events have been studied and empirical formulations have been done to get information about their mass and velocity (Mason et al., 2016). Figure 6 shows the coronal dimming associated with CME due to the solar flare event of 4th August 2011.

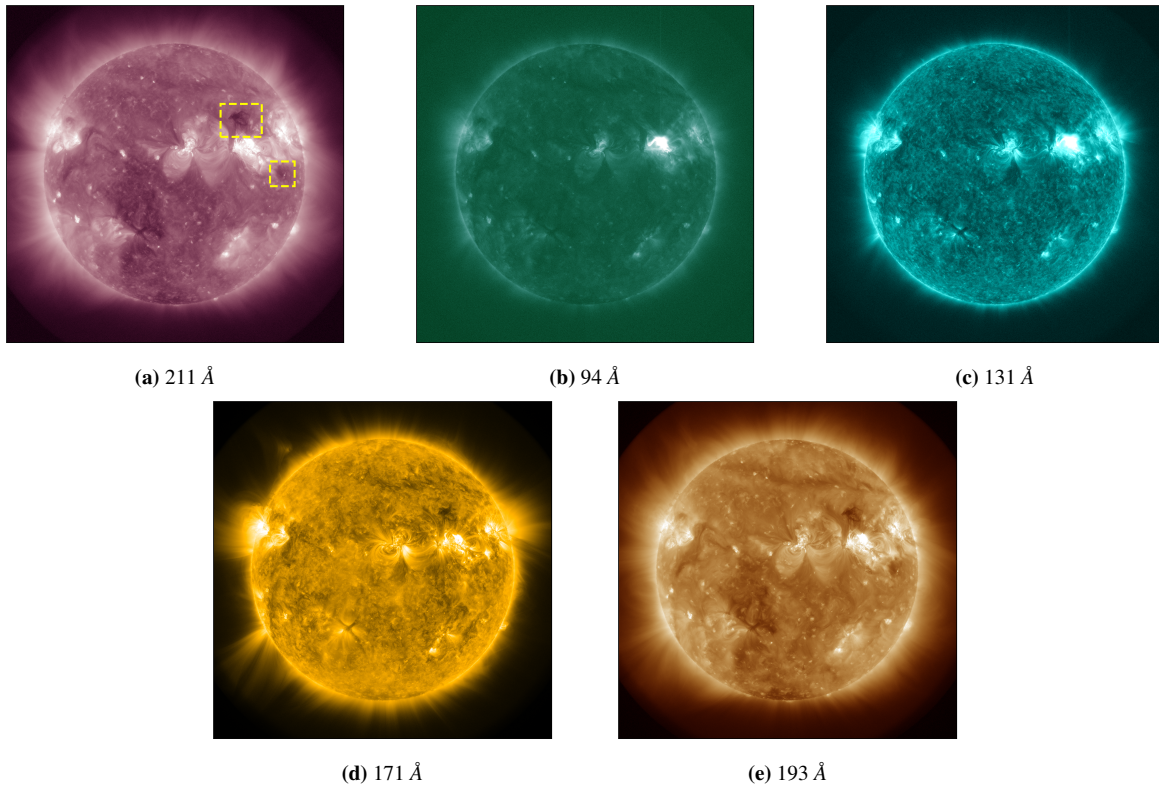


Figure 6: AIA images of the Sun depicting coronal dimming in five of the channels in the order: 211 Å, 94 Å, 131 Å, 171 Å, 193 Å. The two yellow dashed boxes depict the dimming region created because of the ejection of CME associated with the flare event of 4th August 2011 (dimming starts around 04:21 UT).

2.8 Instrument

We are using Atmosphere Imaging Assembly (AIA) instrument of Solar Dynamics Observatory (SDO; (Pesnell et al., 2011))(fig. 7) for the Sun’s spectral irradiance data. SDO is a space observatory launched by NASA on 2010 as a part of ‘Living With a Star’ (LWS) program. The spacecraft contains three instruments on board: Extreme Ultraviolet Variability Experiment (EVE), Helioseismic and Magnetic Imager (HMI), Atmospheric Imaging Assembly (AIA). We’ll be focusing on the AIA instrument, since that is what we are using. AIA was built in partnership with Lockheed Martin Solar and Astrophysics Laboratory (LM-SAL). AIA contains 4 cassegrain telescopes which are optimized to observe narrow bands in the EUV region. Each of the four f/20 telescope has a 20-cm primary mirror and an active secondary mirror. The telescope is designed to prevent charged particles from reaching the

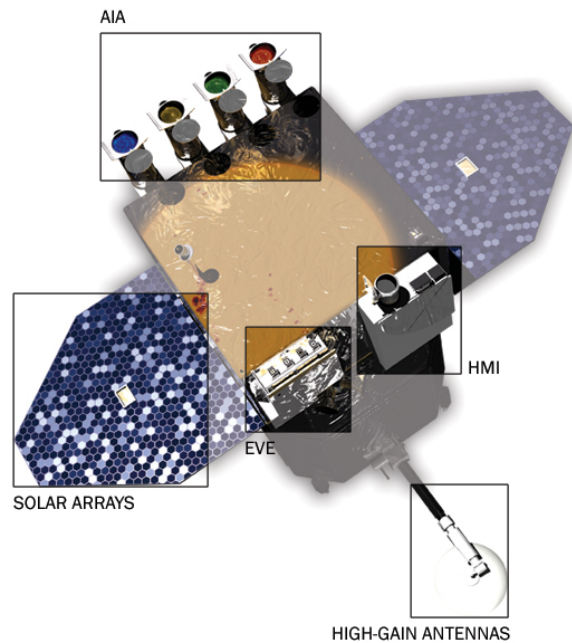


Figure 7: Solar Dynamics Observatory Spacecraft. Image obtained from <https://sdo.gsfc.nasa.gov/mission/spacecraft.php>

Charge Coupled Device (CCD). Field of View (FOV) of each of the telescope is 41 arcmin in circular diameter. The mirrors have special multilayer coatings that are optimized to observe the selected EUV wavelengths of interest. Three of the telescopes have two different EUV bandpasses. The CCDs are back-thinned and back-illuminated with 4096×4096 pixels capturing capabilities. Each of the $12 \mu\text{m}$ pixel corresponds to 0.6 arcsec. The telescopes have a selector mechanism to choose the wavelength. AIA captures full-frame EUV image and one UV or visible-light image every 12 seconds. (Lemen et al., 2011)

The different channels of AIA respond differently to the radiation of different temperature. The channels of AIA along with its primary role, region of Sun's atmosphere it probes and temperature has been given in table 2. The response of the instrument to different wavelengths and temperature is given by its response curves, which are of two types: *wavelength response curve* and *temperature response curves*. Temperature response curves gives the information about the response of each channel with respect to the temperature of the

Band	Primary role, ion(s)	Region of Sun's atmosphere	logT[K]
4500 Å	Continuum	Photosphere	3.7
1700 Å	Continuum	Temperature minimum, photosphere	3.7
304 Å	He II	Chromosphere, transition region	4.7
1600 Å	C IV, continuum	Transition region, upper photosphere	5.0
171 Å	Fe IX	Quiet corona, upper transition region	5.8
193 Å	Fe XII, XXIV	Corona and hot flare plasma	6.1, 7.3
211 Å	Fe XIV	Active region corona	6.3
335 Å	Fe XVI	Active region corona	6.4
94 Å	Fe XVIII	Flaring regions	6.8
131 Å	Fe XX, XXIII	Flaring regions	7.0, 7.2

Table 2: AIA wavelength channels. Table obtained from <https://aia.lmsal.com/public/instrument.htm>

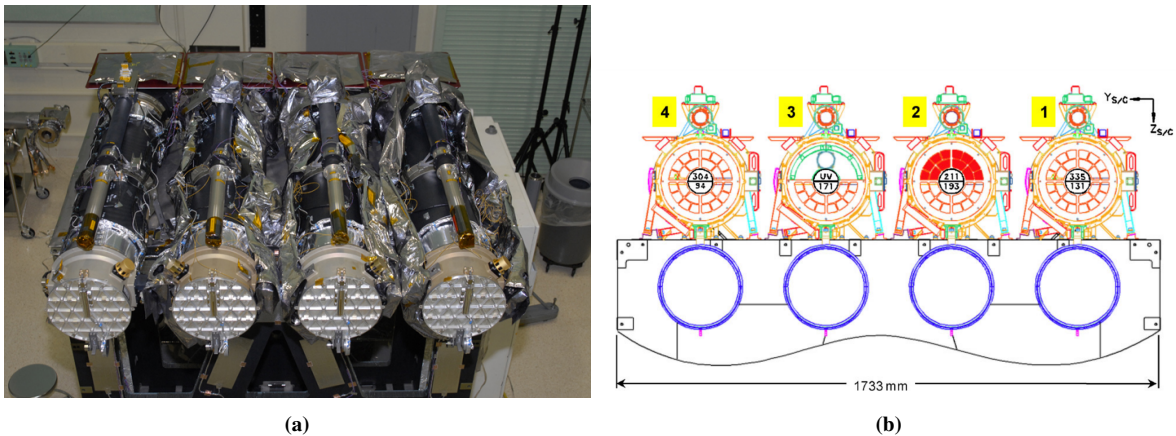


Figure 8: Figure 8a shows the AIA telescopes. Figure 8b shows the AIA telescope layout. Telescope 2 has an aperture blade to select between its two wavelength channels. Rest of the telescopes rely on the filters in filter wheels to select the channel (Image credit: (Lemen et al., 2011))

radiation being received. Temperature response curves play a crucial role in DEM analysis.

Figure 9 shows the response curves, which has been obtained using `aia_get_response.pro` procedure of SSW IDL.

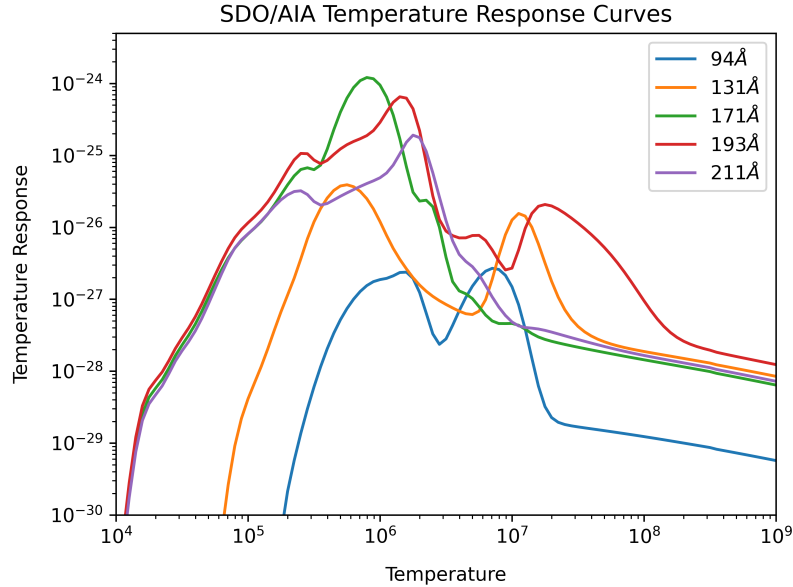


Figure 9: SDO/AIA Temperature Response Curves obtained using `aia_get_response.pro`. Curves corresponding to the five wavelength channels required for the DEM analysis has been plotted. Temperature has the unit of Kelvin and temperature response function has the unit of $[\text{DN cm}^5 \text{s}^{-1} \text{pixel}^{-1}]$

3 Literature Review

The motivation for indirect detection of CMEs from Sun has led researchers to find out association of CMEs with eruptive events on the Sun like Solar flare, filament and prominence eruptions, coronal dimming associations with CME and vice-versa etc. About 73 % association of CME events with eruptive filaments has been observed (Sinha et al., 2019). It has been demonstrated that EM distributions from SDO/AIA data alone can overestimate the amount of high temperature ($\log T > 6.4$) plasma in the solar corona by a factor of 3-15 (Athiray and Winebarger, 2024). Coronal dimming phenomenas have been extensively studied and many empirical formulations have also been derived to get information about the underlying CMEs like mass and velocity of the CMEs ejected by knowing the depth and slope of the dimming curve (Mason et al., 2016). The association of dimming with a CMEs and association of CME with dimming has been observed to be very high ($P(\text{Dim} | \text{CME}) = 0.842$, $P(\text{Dim} | \neg \text{CME}) = 0.167$, $P(\text{CME} | \text{Dim}) = 0.970$) (Veronig et al., 2021). Sun-as-a-star analysis methods have been used widely for comparing and studying

stellar and solar CMEs. Multi-temperature structure analysis of stellar active phenomena in spatially integrated spectra is allowed by the combination of $H\alpha$ and EUV lines, instead of single spectra analysis (Otsu and Asai, 2024). Redshifted components of stellar filament eruptions in Sun-as-a-star analysis in $H\alpha$ spectra may develop into CMEs (Otsu et al., 2022). Further studies into stellar CMEs connecting the CME mass and velocity to the stellar flare energy, leading to the conclusion that stellar CMEs are restricted in terms of their velocity due to the strong stellar magnetic fields and stellar wind drag (Moschou et al., 2019). One expects that the case of stellar CME in terms of its energetics and association to stellar flares will be a scaled version of the solar CMEs, but discrepancy has been found in terms of the ratio between the Kinetic energy of stellar CME to the stellar flaring energy not being anywhere close to being a scaled version of the solar case (Namekata et al., 2022).

4 Methodology

In this study, we use the SDO/AIA data of the Sun for three particular CME events (section 4.2). These events are associated with special features like coronal dimming, filament eruptions and GLE event. The DEM for each image of the three events is obtained using the RML method. Next, we convert the full disk image of Sun to a point source (hereafter referred to as **Pointification**) and then inspecting if the signatures of the CMEs exist after the conversion and is similar to what it was before the conversion. Pointifying the Sun roughly translates to converting Sun to a star, or placing Sun to a place that's distant from Earth/observer in comparison to the distance between us and the Sun (defined as astronomical unit ($1 \text{ AU} \approx 1.496 \times 10^8 \text{ km}$)) such that it appears as a point source. We then analyse and compare the irradiance from the point source Sun and the full disk Sun using DEM to see if they show similar signatures of CMEs. Typically, Sun-as-a-star analysis involves selecting a region of interest on the surface of the Sun, making the assumption that this is the only region that affects the event under study, and that there is no activity anywhere on the rest of the Sun's surface, and then integrating the parameter of interest over the entire Solar disk. This is again a rough approximation to an actual star. Coronal dimming associated event is

investigated to find the temperature range that shows the maximum amount of dimming.

In the following section, we discuss about the analysis tools used (section 4.1), selection of events (section 4.2), data used for the study (section 4.3), data pre-processing (section 4.4) and data analysis procedure (section 4.6).

4.1 Data Analysis tools used

We have made use of Python programming language for our analysis. We have made extensive use of the following libraries: Numpy, Scipy, Aiapy, Sunpy, Pandas, Matplotlib, Astropy, Natsort, Multiprocessing, Datetime, Moviepy. In addition, we have used the RML method code for DEM analysis, as mentioned in (Massa et al., 2023). We have made use of SSW IDL for obtaining the temperature response curves for AIA. For visual inspection of the CME events, we have used JHelioViewer software. For quick inspection of the FITS file data, we have used FITSExplorer¹, a software created as a side project by D. V. Shenoy.

4.2 Event Selection

We have chosen three CME events that have erupted on 2011 August 04, 2012 August 31 and 2021 October 28. The Solar and Heliospheric Observatory's (SOHO) Large Angle and Spectrometric Coronagraph Experiment (LASCO) C2 (SOHO/LASCO) images of the CMEs obtained from the SOHO/LASCO CME catalog (https://cdaw.gsfc.nasa.gov/CME_list/) are given in fig. 11 and fig. 12. Brief description of the events is given below:

1. **2011 August 04:** This event has been referred from (Mason et al., 2016) in which it is the 20th Event. The event started at around 04:12 UT. This event occurred from the source location N19W36 associated with the active region AR 11261.
2. **2012 August 31:** This CME event was associated with a long filament eruption and it erupted around 19:49 UT. The CME associated with the filament travelled at over 900

¹link to the github repo: <https://github.com/dheerajshenoy/FITSExplorer>

miles per second.

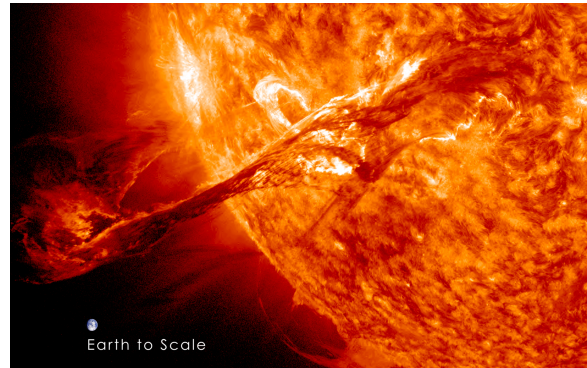


Figure 10: Image of the Earth to scale with the filament eruption of 31st August 2012. Image credit: <https://svs.gsfc.nasa.gov/11095>

3. **2021 October 28:** This is an example for rarely occurring ‘ground level enhancement’ event. During such an event, particles from the Sun are energetic enough to pass through the magnetic sheath that surrounds Earth and protects us from low energy solar outbursts. This was only the 73rd ground level enhancement since records began in the 1940s, and none have been recorded since (Klein et al., 2022). The event occurred around 15:17 UT. The flare associated with the CME was an X1.1 class flare originated from the active region AR 2887.

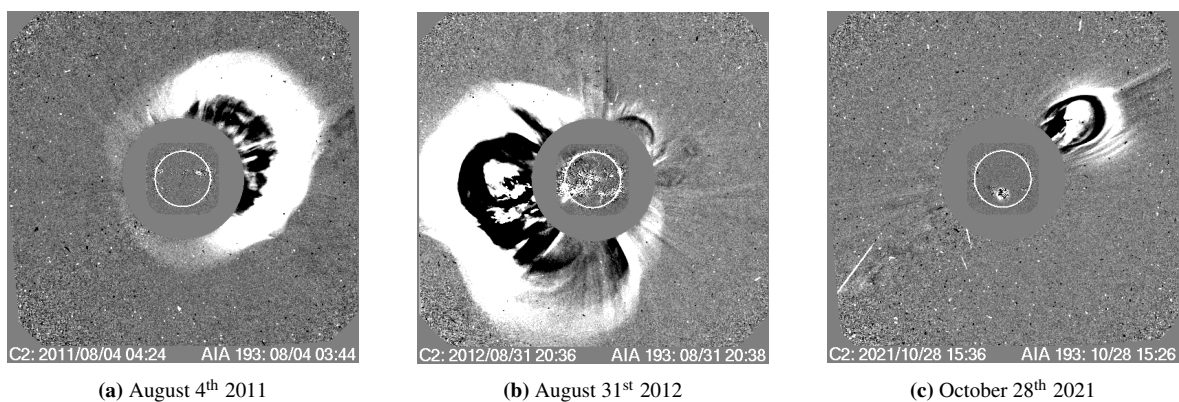


Figure 11: SOHO/LASCO C2 running difference images of the three selected events

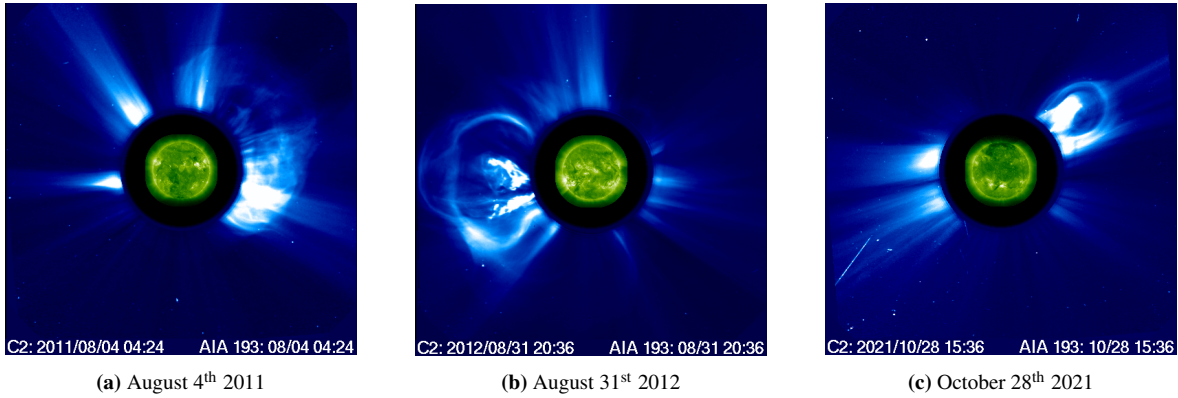


Figure 12: SOHO/LASCO C2 AIA 193 Å filter images of the three selected events

4.3 Data

The SDO/AIA data is accessed through the JSOC portal (<http://jsoc.stanford.edu>) and required event data is obtained through the service. Event data consists of FITS files of Sun's image for the selected wavelength bands. For our analysis, we have used 5 channels: 94 Å, 131 Å, 171 Å, 193 Å and 211 Å. The remaining channels probe the Sun's surface temperature that is greater than what is required for our analysis. Also, the 335 Å channel has been excluded because of its relatively weak temperature response at any temperature which affects the RML method used for the DEM analysis (Massa et al., 2023). We have used 10 hours of data for the 4th August 2011 and 31st August 2012 events, and about 7 hours of data for the 28th October 2021 event. All three event data are at 2 minute cadence (Cadence refers to the frequency or timing of observations or measurements taken of the Sun or solar phenomena. It represents how often data is collected over a period of time).

4.4 Image Pre-Processing

The downloaded FITS data files are 4096×4096 pixels in dimension. Data downloaded from the portal is level 1, which has been flat-fielded and processed to remove bad pixels and spikes (only for EUV channels), but not registered to preserve precise pixel values. As different channels of AIA have different roll angles, multi-wavelength analysis of any kind with level 1.0 data is problematic. Also, the pointing information contained in the headers of

these FITS images will not be accurate, as it would have undergone changes compared to the information stored when the image was created. As mentioned in the SDO Data Analysis Guide, we have to use `aia_prep.pro` function in Solar Software (SSW) IDL to correct or prepare the data used. Additionally, the images are downsampled from their original 4096×4096 pixel dimension to 512×512 pixels using `sunpy` as obtaining DEM solutions for the 4k dimension would be really time consuming and unnecessary as we are comparing full disk and point source DEM solutions.

The `aiapy` library is used to carry out the necessary procedure like ‘**Pointing correction**’ and ‘**Registration**’ as mentioned in the documentation of `aiapy`, to convert level 1 data to level 1.5. Pointing correction updates the keywords in the header of the FITS file to the latest information and Registration rotates, scales and translates the image so that the Solar north is aligned with the solar north and each pixel is 0.6 arcsec cross, and the center of the Sun is at the center of the image. Now, after this calibration, the images are good for multi-wavelength analysis. Finally, the images are normalized with respect to their exposure time. This is done because the images are captured under different lighting conditions or exposure settings, which leads to incorrect analysis when performing a multi-wavelength comparison. Without this, differences in brightness due to varying exposure times could distort interpretations and analysis.

4.5 DEM Analysis

Direct analysis of light curve might seem like a good choice as the effects of CMEs are seen in light curves too. But, light curve alone doesn’t have any information about the temperature of the plasma that is being expelled. Information regarding the temperature can be derived using Differential Emission Measure (DEM) solutions obtained using the images of Sun. This allows us to understand the plasma temperature variations during eruptive events.

4.5.1 Emission Measure

Emission measure (EM) is a quantity used in astrophysics to describe the amount of emitting material along the line of sight in a particular volume, usually in the context of a hot or ionized gas, such as a stellar atmosphere. It provides a measure of the emission intensity of a given region at various temperatures. It is expressed in units of cm^{-3} or cm^{-5} , representing the number of electrons emitting radiation per unit volume or per unit area, respectively.

Emission measure is related to the number density of electrons $n_e(T)$ at a particular temperature T , in a volume dV of plasma, in a particular temperature range T_1 and T_2 , along the line of sight, given by,

$$EM = \int_{T_1}^{T_2} n_e^2(T) dV \quad (1)$$

Emission measure is a crucial parameter in understanding the energetics and physical conditions of a plasma, such as those found in stars, galaxies and other astrophysical environments. In the context of the Sun, the emission measure is often used to study the solar corona, helping us to understand the distribution of temperatures and the processes governing the heating of the outer solar atmosphere.

4.5.2 Differential Emission Measure

Differential Emission Measure (DEM) is used to describe the distribution of emitting material at different temperatures in a given volume. It is a measurement of the amount of plasma at various temperatures per unit volume along the sight. DEM helps us understand how much material is present at different temperature in stellar atmosphere. This is crucial for studying the physical conditions and processes occurring in stellar atmospheres. DEM is usually expressed in units of $cm^{-5}K^{-1}$, representing the number of particles emitting radiation at a particular temperature per unit volume.

$$DEM = f(T) = \frac{d}{dT} EM = n_e^2(T) \frac{dV}{dT} \quad (2)$$

The integral of $DEM(T)$ over a finite temperature range is called as the emission measure. This quantity helps to understand the thermal structure of a stellar atmosphere, providing insight into the distribution of temperatures and the heating mechanisms that operate in a particular region. DEM arises from certain aspects of coronal emission line. Optically thin property of corona, scaling of emission line intensity with density squared $n_e(T)^2$ (for most lines) and temperature response function $K(T)$ that peaks at certain temperature for each of the lines. If $K_i(T)$ is the temperature response function of a particular channel, then the count-rate y_i of the i^{th} EUV channel is related to the temperature distribution of coronal plasma as,

$$y_i = \int_0^\infty K_i(T) DEM(T) dT \quad (3)$$

where

$$DEM(T)dT = \int_0^\infty n_e^2(T)dV \quad (4)$$

From DEM , parameters like plasma density, thermal X-ray flux, thermal energy and weighted temperature emission measure etc. can be estimated (Su et al., 2018). In solar research, DEM aids in understanding the Sun's atmosphere, while in stellar astrophysics, it contributes to characterizing other stars, enhancing our knowledge of stellar diversity and evolution (Namekata et al., 2023).

4.5.3 Differential Emission Measure Inversion

DEM inversion refers to the process of determining the physical conditions of the plasma from observed coronal emission line data. The challenge is simply to solve eq. (3) for $DEM(T)$ given a set of measurements y . Radiation emitted by the plasma is observed at different wavelengths using spectroscopic techniques. The observed data is then used to con-

struct the DEM, which represents the distribution of emitting material at different temperatures in the stellar atmosphere. Next, the inversion process is employed, which is basically reconstructing the DEM, thereby helping us to determine the underlying temperature distribution which gave rise to the observed emission line intensities. Then different computational techniques can be employed to fit theoretical models of the emission at different temperatures to the observed data. The best fit model then provides the information about the temperature distribution of the plasma.

Many DEM inversion techniques have been developed over the years: basis pursuit technique (**Cheung et al., 2015**), fast iterative regularized method (**Plowman et al., 2013**), iterative SITES method (**Morgan and Pickering, 2019**), regularized method (REG) (**Hannah and Kontar, 2012**), regularized maximum likelihood (RML) method (**Massa et al., 2023**) etc. We will be making use of the RML method, as it has been found to be a good approximation to the actual DEM profiles and is performant in comparison to the other methods.

4.6 Data Analysis Procedure

After calibration (registering, pointing correction and exposure time normalization), the image data is fed to the RML code (**2023**) which returns the DEM solutions for the desired temperature range. We choose a temperature (logarithm) range of $\log T[\text{K}] = [5.85, 6.75]$ which translates to temperature of $10^{5.85} \approx 7 \times 10^5 K$ to $10^{6.75} \approx 5.6 \times 10^6 K$. The function `rml_dem` takes the following inputs: array containing the AIA data (DN/s), array of uncertainties of AIA data (DN/s), exposure time value for each AIA channel (s), array containing the temperature response function for each channel ($DN\text{ cm}^5\text{ pixel}^{-1}\text{ s}^{-1}$), array containing the value of log base 10 of the center of each temperature bin, array containing the value of the width of base 10 logarithm of the temperature bins. The function returns an array containing the values of the reconstructed DEM profiles. The returned solutions will be spaced according the temperature spacing of the response function array fed to the solver. The solutions obtained can be plotted to look at the emission measure distribution as shown in fig. 13.

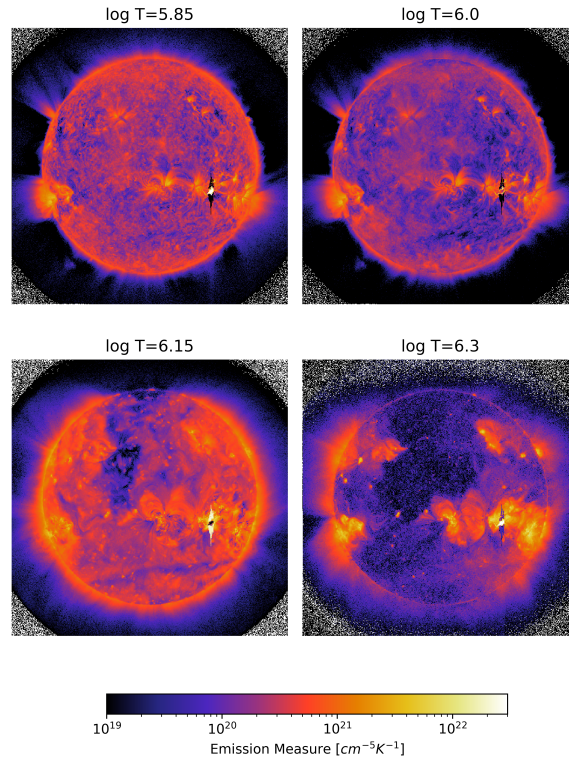


Figure 13: DEM of Sun during the flaring event on 4th August 2011. The artifacts at the corners of the image is due to the diffraction of light in the telescope of AIA

Next step is to generate the point source from the full disk, which we refer to as “Pointification”. This involves the conversion of the full disk image of Sun to a point source, which mimics a distant star. The original image of 4096×4096 pixels dimension is averaged and new image having 512×512 pixels dimension is created with the pixel value at (256, 256) of the image (midpoint of the image) equal to the calculated average image pixel value. The average values of 4096×4096 pixel image dimension has been considered and not the 512 one so as to not allow the errors due to the resampling of the image affect the average pixel intensity value significantly. Figure 14 shows the result of pointification procedure. After pointification, DEM profile is reconstructed from these images. These act like DEM profiles of a point source/star.

The temperature $\log T$ can be grouped into discrete ranges with the corresponding dem

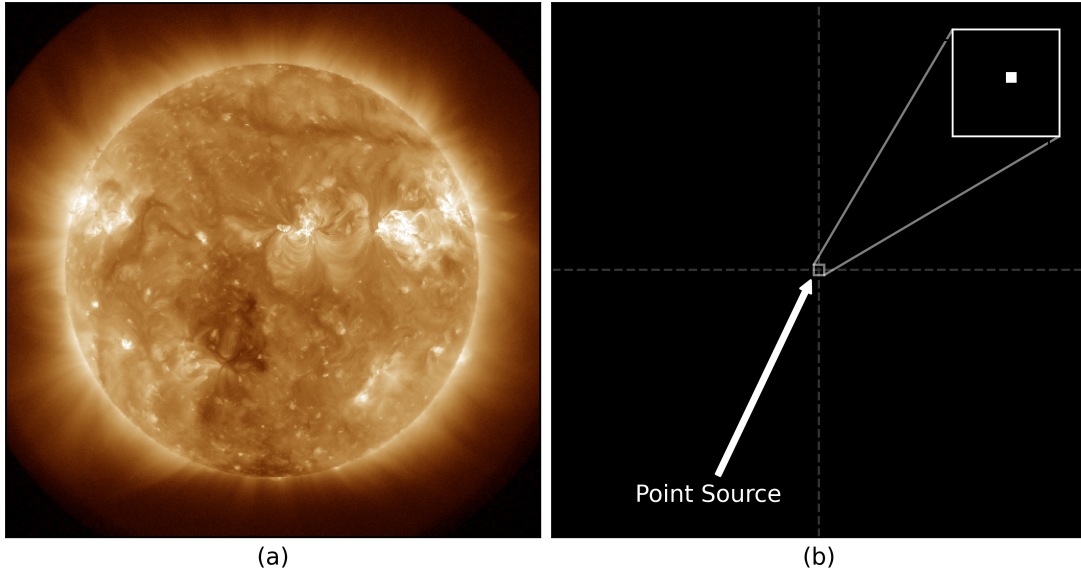


Figure 14: (a) shows the full disk image of Sun in the 193 Å channel, (b) shows the image after pointification.

solutions being group by averaging. The grouping interval depends on the temperature interval used for the analysis, which in our case is 0.15 K. We have grouped three consecutive temperature intervals (eg: 5.85, 6.0, 6.15). This is called as temperature binning. Binning helps in reducing the impact of noise or uncertainties in the data. By averaging the emission measurements for each temperature bin, we can smoothen fluctuations and obtain a good estimate of the DEM.

5 Results

Figure 15, fig. 16 and fig. 17 shows the timeseries plot of DEM for the three events. The time series plot is calculated by averaging the acceptable DEM solutions obtained for each image over three consecutive temperature range (i.e averaging the solutions for 5.85, 5.9 and 5.95 etc.). Blue curve corresponds to the full disk DEM and red curve corresponds to the point source DEM. The temperature range above $\log T=6.75$ has been omitted as no correlation was found between point source and full disk.

In fig. 15(a) and fig. 15(b), we can observe the coronal dimming or decrease in the

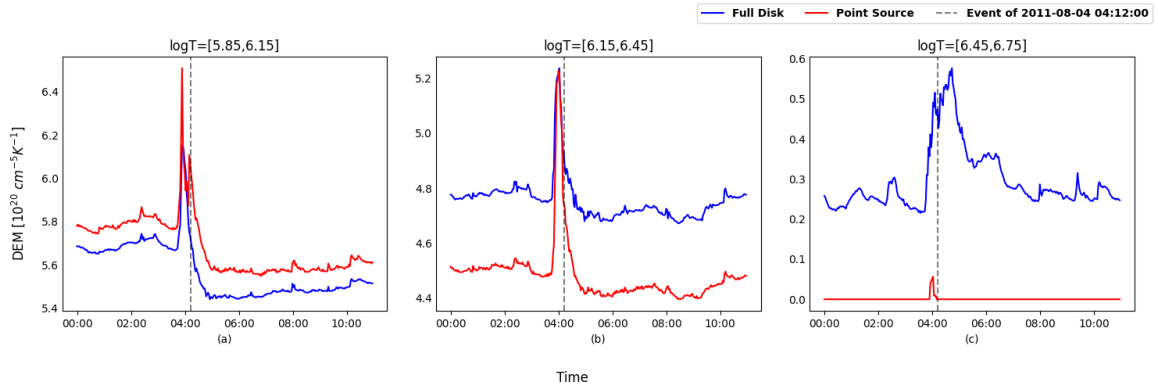


Figure 15: Timeseries of DEM for 4th August 2011 Event.

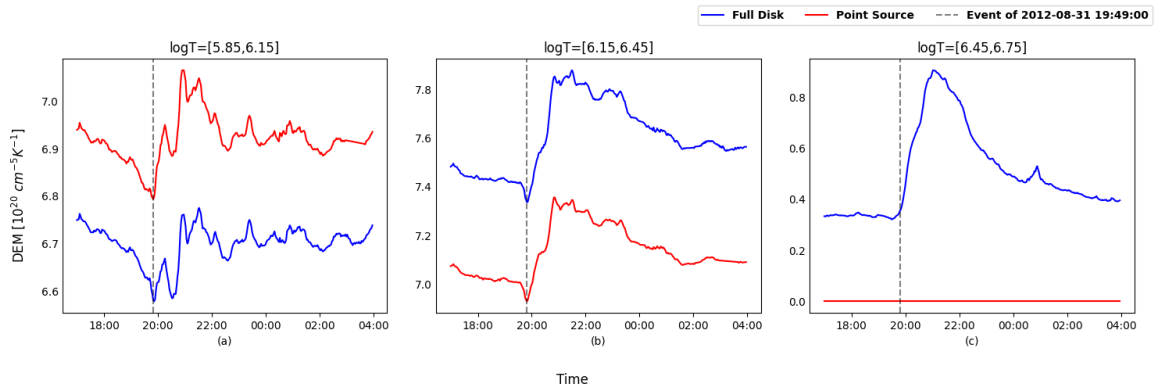


Figure 16: Timeseries of DEM for 31st August 2012 Event

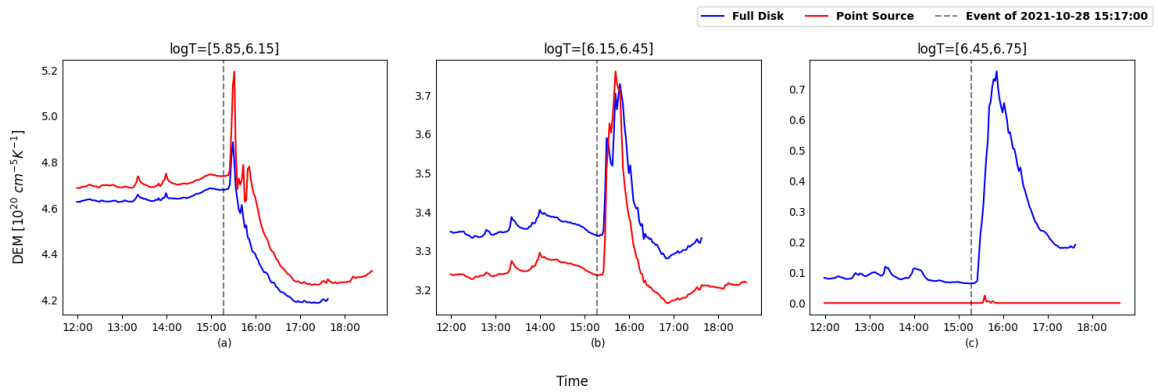


Figure 17: Timeseries of DEM for 28th October 2021 Event

DEM value after the event spike. But, in fig. 15(c) no dimming is observed. Dimming is the most prominent in $\log T = [5.85, 6.15]$. This means that the mass loss of coronal plasma is mostly seen in this temperature range. The sudden increase in the DEM curve is due to

the solar flare which is associated with the CME. There is very high correlation for the first two temperature ranges, but there is little to no correlation in the DEM profiles of the full disk and point source for the temperature range $\log T = [6.45, 6.75]$. For temperature ranges greater than $\log T = 6.45$, the correlation is almost 0. We make use of Pearson's Correlation coefficient (eq. (5)) to find out the amount of correlation between the point source and full disk DEM, for which we use `pearsonr` function from the `scipy` library in Python. The pearson correlation coefficient r between two datasets \mathbf{x} and \mathbf{y} is calculated using the formula,

$$r = \frac{\sum(x_i - \bar{x})(y_i - \bar{y})}{\sqrt{\sum(x_i - \bar{x})^2 \sum(y_i - \bar{y})^2}} \quad (5)$$

Event	Pearson Correlation Coefficient		
	$\log T = [5.85, 6.15]$	$\log T = [6.15, 6.45]$	$\log T = [6.45, 6.75]$
4 th August 2011	0.9449	0.9767	0.2190
31 st August 2012	0.7027	0.9885	0.2079
28 th October 2021	0.9555	0.9577	0.2578

Table 3: Correlation between Point source and Full Disk DEM

The correlation in the DEM curves of the point source and full disk below $\log T \leq 6.45$ means that point source image of Sun shows characteristic behaviours like coronal dimming associated with the CMEs, filament eruption associated CMEs and GLE CME signatures seen in the case of full disk image of Sun.

We see a discrepancy in the value of DEM between the point source and full disk average values. This could be due to the error induced during the DEM profile reconstruction, instrumental and averaging error. As seen in fig. 13, the noise pixels in the corners of the image, due to the diffraction of light with the AIA telescopes, affect the pointification process, inducing high errors. The dataset length is not equal in some of the case as invalid or small DEM solution values have been removed.

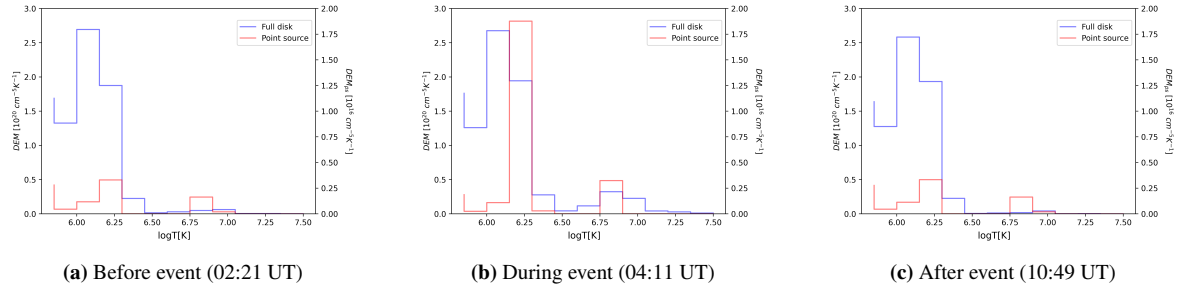


Figure 18: DEM profile before, during and after the flaring event of 4th August 2011. The red and blue curves correspond to point source and full disk source respectively. DEM_{ps} represents the DEM of the point source.

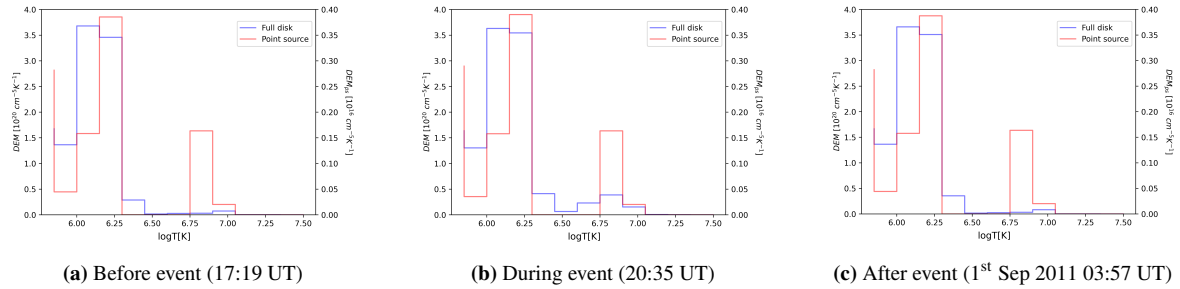


Figure 19: DEM profile before, during and after the flaring event of 31st August 2012.

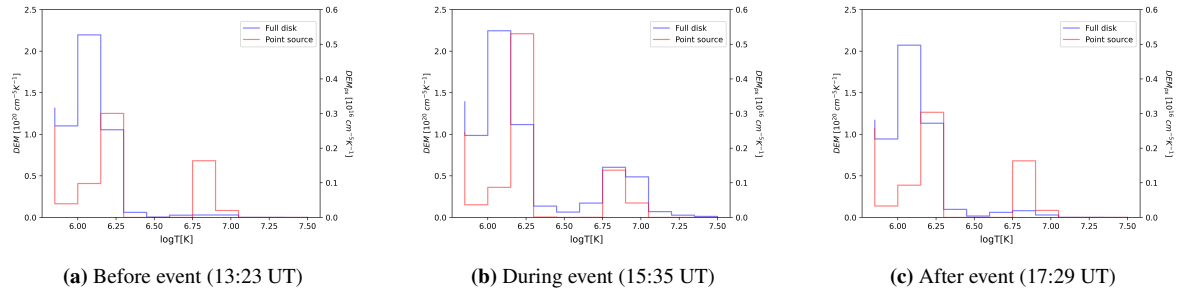


Figure 20: DEM profile before, during and after the flaring event of 28th October 2021.

The temperature distribution of the plasma at different sections of an event can be studied through its DEM profile (DEM profile is a plot of $\log T$ vs DEM). The DEM profiles before, during and after the event has been shown in fig. 18, fig. 19 and fig. 20 for the events of 4th August 2011, 31st August 2012 and 28th October 2021 respectively.

In fig. 18 and fig. 19 the DEM profile (full disk + point source) before and after the event looks similar. Figure 18b shows the increase in full disk emission during the event in

the range $\log T \sim [6.5, 7.0]$ and point source emission increases in the range $\log T \sim [6.125, 6.25]$. Figure 19b shows a slight increase in the full disk emission in the range $\log T \sim [6.6, 7.0]$, but not change in the point source DEM is observed.

Figure 20 shows increase in emission of full disk in the range $\log T \sim [6.25, 7.25]$ during the event. But, there is slight increase in the emission in this range after the event (compared to before the event), which is not observed in the previous two events.

6 Discussion and Conclusion

In this study, we have presented a comprehensive analysis of CMEs on the Sun through DEM analysis, incorporating innovative methodologies and novel approaches. We have analyzed three CME events, each associated with unique solar phenomena like coronal dimming, filament eruption and ground level enhancement CME event. Our DEM analysis shows that the maximum dimming depth temperature range for the event of 4th August 2011 has been seen in the range $\log T = [5.85, 6.15]$, shedding light into the underlying physical mechanisms driving dimming phenomena. We demonstrated the process of converting full disk image to a point source, to study the Sun-star CME relation. The correlation between the full disk and point source DEM is high in the temperature range below $\log T \sim 6.45$. Discrepancy in the value of DEM is observed between the point source and the full disk which might be because of many reasons like naively averaging the entire image when reducing to a point source, error in the DEM inversion.

The pointification of the full disk image has rooms for improvement, which has to be taken care of during further studies. Approach like naively directly averaging the pixel values of images and reduction to point source poses problems at places where the corresponding DEM solutions either do not exist or is very minute in the full disk image, leading to incorrect averaging of pixels for the case of point source. Hence, careful reduction to point source is necessary. Moving forward, we plan to improve the point source reduction process, increase the temperature interval to increase the accuracy of the DEM solutions and look at

more events, so that we can do a statistical analysis, which would enable us to check if the correlations observed actually hold for a larger set of events. Additionally, we also would look at CME events originating at different regions on the Sun and understand its effect on the coronal dimming and temperature variations of the Solar corona.

References

- Argiroffi, C., Reale, F., Drake, J. J., Ciaravella, A., Testa, P., Bonito, R., Miceli, M., Orlando, S., & Peres, G. (2019). A stellar flarecoronal mass ejection event revealed by x-ray plasma motions. *Nature Astronomy*, 3(8), 742–748. <https://doi.org/10.1038/s41550-019-0781-4>
- Aschwanden, M. (2006). *Physics of the solar corona: An introduction with problems and solutions*. Springer Berlin Heidelberg.
- Athiray, P. S., & Winebarger, A. R. (2024). Can emission measure distributions derived from extreme-ultraviolet images accurately constrain high-temperature plasma? *The Astrophysical Journal*, 961(2), 181. <https://doi.org/10.3847/1538-4357/ad1837>
- Cheung, M. C. M., Boerner, P., Schrijver, C. J., Testa, P., Chen, F., Peter, H., & Malanushenko, A. (2015). Thermal diagnostics with the atmospheric imaging assembly on board the solar dynamics observatory: A validated method for differential emission measure inversions. *The Astrophysical Journal*, 807(2), 143. <https://doi.org/10.1088/0004-637x/807/2/143>
- Gopalswamy, N. (2016). History and development of coronal mass ejections as a key player in solar terrestrial relationship. *Geosci. Lett.*, 3(1).
- Hannah, I. G., & Kontar, E. P. (2012). Differential emission measures from the regularized inversion of hinode and sdo data. *Astronomy & Astrophysics*, 539, A146. <https://doi.org/10.1051/0004-6361/201117576>
- Klein, K.-L., Musset, S., Vilmer, N., Briand, C., Krucker, S., Francesco Battaglia, A., Dresing, N., Palmroos, C., & Gary, D. E. (2022). The relativistic solar particle event on 28 october 2021: Evidence of particle acceleration within and escape from the solar corona. *Astronomy & Astrophysics*, 663, A173. <https://doi.org/10.1051/0004-6361/202243903>
- Korhonen, H., Vida, K., Leitzinger, M., Odert, P., & Kovacs, O. E. (2016). Hunting for stellar coronal mass ejections.
- Lemen, J. R., Title, A. M., Akin, D. J., Boerner, P. F., Chou, C., Drake, J. F., Duncan, D. W., Edwards, C. G., Friedlaender, F. M., Heyman, G. F., Hurlburt, N. E., Katz, N. L., Kushner, G. D., Levay, M., Lindgren, R. W., Mathur, D. P., McFeaters, E. L., Mitchell, S., Rehse, R. A., ... Waltham, N. (2011). The

- atmospheric imaging assembly (aia) on the solar dynamics observatory (sdo). *Solar Physics*, 275(1–2), 17–40. <https://doi.org/10.1007/s11207-011-9776-8>
- Mason, J. P., Woods, T. N., Caspi, A., Thompson, B. J., & Hock, R. A. (2014). Mechanisms and observations of coronal dimming for the 2010 august 7 event. *The Astrophysical Journal*, 789(1), 61. <https://doi.org/10.1088/0004-637x/789/1/61>
- Mason, J. P., Woods, T. N., Webb, D. F., Thompson, B. J., Colaninno, R. C., & Vourlidas, A. (2016). Relationship of euV irradiance coronal dimming slope and depth to coronal mass ejection speed and mass. *Astrophys. J.*, 830(1), 20.
- Massa, P., Emslie, A. G., Hannah, I. G., & Kontar, E. P. (2023). Robust construction of differential emission measure profiles using a regularized maximum likelihood method. *Astronomy & Astrophysics*, 672, A120. <https://doi.org/10.1051/0004-6361/202345883>
- Morgan, H., & Pickering, J. (2019). Sites: Solar iterative temperature emission solver for differential emission measure inversion of euV observations. *Solar Physics*, 294(10). <https://doi.org/10.1007/s11207-019-1525-4>
- Moschou, S.-P., Drake, J. J., Cohen, O., Alvarado-Gómez, J. D., Garraffo, C., & Fraschetti, F. (2019). The stellar CME–flare relation: What do historic observations reveal? *Astrophys. J.*, 877(2), 105.
- Namekata, K., Maehara, H., Honda, S., Notsu, Y., Nogami, D., & Shibata, K. (2022). Hunting for stellar coronal mass ejections.
- Namekata, K., Toriumi, S., Airapetian, V. S., Shoda, M., Watanabe, K., & Notsu, Y. (2023). Reconstructing the XUV spectra of active sun-like stars using solar scaling relations with magnetic flux. *Astrophys. J.*, 945(2), 147.
- Otsu, T., & Asai, A. (2024). Multiwavelength sun-as-a-star analysis of the m8.7 flare on 2022 october 2 using h and euV spectra taken by smart/sddi and sdo/eve. *The Astrophysical Journal*, 964(1), 75. <https://doi.org/10.3847/1538-4357/ad24ec>
- Otsu, T., Asai, A., Ichimoto, K., Ishii, T. T., & Namekata, K. (2022). Sun-as-a-star analyses of various solar active events using h spectral images taken by smart/sddi. *The Astrophysical Journal*, 939(2), 98. <https://doi.org/10.3847/1538-4357/ac9730>
- Pesnell, W. D., Thompson, B. J., & Chamberlin, P. C. (2011). The solar dynamics observatory (sdo). *Solar Physics*, 275(1–2), 3–15. <https://doi.org/10.1007/s11207-011-9841-3>
- Plowman, J., Kankelborg, C., & Martens, P. (2013). Fast differential emission measure inversion of solar coronal data. *The Astrophysical Journal*, 771(1), 2. <https://doi.org/10.1088/0004-637x/771/1/2>
- Sinha, S., Srivastava, N., & Nandy, D. (2019). Solar filament eruptions as precursors to flare–cme events: Establishing the temporal connection. *The Astrophysical Journal*, 880(2), 84. <https://doi.org/10.3847/1538-4357/ab2239>

-
- Su, Y., Veronig, A. M., Hannah, I. G., Cheung, M. C. M., Dennis, B. R., Holman, G. D., Gan, W., & Li, Y. (2018). Determination of differential emission measure from solar extreme ultraviolet images. *Astrophys. J. Lett.*, 856(1), L17.
- Veronig, A. M., Odert, P., Leitzinger, M., Dissauer, K., Fleck, N. C., & Hudson, H. S. (2021). Indications of stellar coronal mass ejections through coronal dimmings.